High-Efficiency Organic Solar Cells enabled by Nonfullerene Acceptors with Varying Alkyloxy Substitution Position of phenyl Outer Side Chains

Huanran Feng‡[a*], Changzun Jiang‡[b], ZhiXiang Li[b], Xiangjian Wan[b], Bin Kan[c*], and Yongsheng Chen[b]

[a]Interdisciplinary Research Center of Smart Sensors, Shaanxi Key Laboratory of High-Orbits-Electron Materials and Protection Technology for Aerospace, School of Advanced Materials and Nanotechnology, Xidian University, Shaanxi, 710126, People's Republic of China

[b]State Key Laboratory of Elemento- Organic Chemistry, The Centre of Nanoscale Science and Technology and Key Laboratory of Functional Polymer Materials, Institute of Polymer Chemistry, College of Chemistry, Haihe Laboratory of Sustainable Chemical Transformations, Renewable Energy Conversion and Storage Center (RECAST), Nankai University, 300071, Tianjin, China.

[c]School of Materials Science and Engineering, National Institute for Advanced Materials, Nankai University, 300350, Tianjin, China.

‡ These authors contributed equally to this work.

* Corresponding E-mails: hrfeng@xidian.edu.cn (H. F.); kanbin04@nankai.edu.cn (B. K.)

Content

1. Measurements and Instruments

2. Materials Synthesis and Characterization

3. Device Fabrication

4. Figures and Tables

5. NMR Spectra

6. High-Resolution Mass Spectra

7. References

1. Measurements and Instruments

The 1H, 13C nuclear magnetic resonance (NMR) spectra were taken on a Bruker AV400 Spectrometer. Matrix-assisted laser desorption/ionization time-of-flight (MALDI-TOF) mass spectrometry was performed on a Bruker Autoflex III instrument. Fourier transform mass spectrometry (FTMS) with high-resolution matrix-assisted laser desorption/ionization (HR-MALDI) was performed on a Varian 7.0T FTMS instrument. Ultraviolet-visible (UV-Vis) absorption spectra were measured on a UV-Vis instrument Agilent Cary 5000 UV-Vis-NIR spectrophotometer.

Cyclic voltammetry (CV) experiments were employed to evaluate the energy levels with an LK98B II Microcomputer-based Electrochemical Analyzer in acetonitrile solution at room temperature. The experiments were carried out in a conventional three-electrode configuration with a glassy carbon electrode as the working electrode, a saturated calomel electrode (SCE) as the reference electrode and a Pt wire as the counter electrode. Tetrabutylammonium phosphorus hexafluoride (Bu_4NPF_6, 0.1 M) in dry acetonitrile solution was used as the supporting electrolyte with the scan rate of 100 mV/s under the protection of nitrogen. The highest occupied molecular orbital (HOMO) and lowest unoccupied molecular orbital (LUMO) energy levels were calculated from the onset oxidation potential and the onset reduction potential, using the equation $EHOMO = -(4.80+E_{ox}^{onset})$, $ELUMO = -(4.80+E_{red}^{onset})$.

The current density-voltage (*J*-V) curves of photovoltaic devices were recorded by a Keithley 2400 source-measure unit. The photocurrent was measured under the simulated illumination of 100 mW cm^{-2} with AM 1.5 G using a Enli SS-F5-3A solar simulator, which was calibrated by a standard Si solar cell (made by Enli Technology Co., Ltd., Taiwan, and calibrated report can be traced to NREL). The thickness of the active layers was measured by a Veeco

Dektak 150 profilometer. The EQE spectra were measured by using a QE-R Solar Cell Spectral Response Measurement System (Enli Technology Co., Ltd., Taiwan). The FTPS-EQE measurement was carried out on an Enlitech FTPS PECT-600 instrument. The operation stability tests were carried out on a commercial test system (PAS-GV, Enli Technology Co., Ltd., Taiwan). Continuous illumination was provided by an array of LED at 25 ± 2 °C. The performance evolution of devices was tracked under max power point in a glovebox filled with ultrahigh purity nitrogen (<0.1 ppm O_2 and H_2O) without encapsulation.

Atomic force microscope (AFM) investigation was performed using Bruker MultiMode 8 in tapping mode. The GIWAXS data were obtained at 1W1A Diffuse X-ray Scattering Station, Beijing Synchrotron Radiation Facility (BSRF-1W1A). The grazing incident angle was 0.2 degree, and the exposure time was 60 seconds. The geometry structures of molecules were optimized by using DFT calculations (B3LYP/6-31G(d, p)), and the frequency analysis was followed to assure that the optimized structures were stable states. All calculations were carried out using Gaussian 09.

The hole and electron mobility were measured using the space charge limited current (SCLC) method, employing a diode configuration of ITO/PEDOT:PSS/PM6:p-BTP-OEH (94 nm) or PM6:m-BTP-OEH (98 nm) /MoO_x/Ag for holes and ITO/ZnO/PFN-Br/ PM6:p-BTP-OEH (95 nm) or PM6:m-BTP-OEH (93 nm)/PDNIT-F3N/Ag for electrons by taking the dark current density and fitting the results to a space charge limited form, where SCLC is described by:

$$J = \frac{9\varepsilon_0\varepsilon_r\mu_0 V^2}{8L^3}$$

where J is the current density, L is the film thickness of the active layer, μ is the hole or electron mobility, ε_r is the relative dielectric constant of the transport medium, ε_0 is the permittivity of free space (8.85×10^{-12} F m^{-1}), V ($=V_{appl} - V_{bi}$) is the internal voltage in the device, where V_{appl} is the applied voltage to the device and V_{bi} is the built-in voltage due to the relative work function difference of the two electrodes.

TPV and TPC measurements. A white light bias was generated from an array of diodes (Molex 180081-4320) with light intensity about 0.5 sun. A diode pumped laser (Lapa-80) was used as the perturbation source, with a pulse duration of 10 ns and a repetition frequency of 20 Hz. Voltage and current dynamics were recorded on a digital oscilloscope (Tektronix MDO4104C), and voltages at open circuit and currents under short circuit conditions were measured over a 1 MΩ and a 50 Ω resistor, respectively.

2. Materials Synthesis and Characterization

Materials and synthesis. Donor polymer PM6 was purchased from Solarmer Materials, Inc. TPBT-2Br was prepared according to the literature.[1] The solvents were purified and dried according to standard procedures. The other materials were common commercial level and used as received.

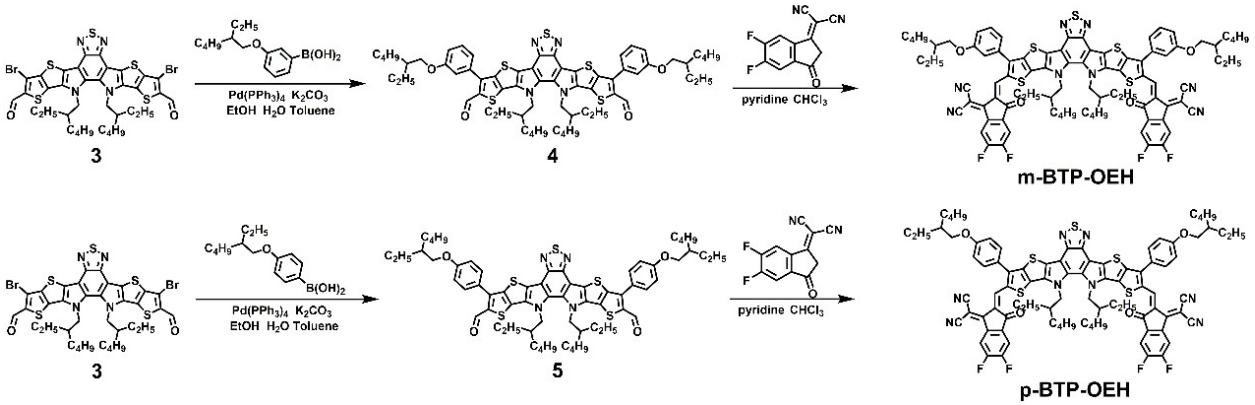

Figure S1. Synthetic route of m-BTP-OEH and p-BTP-OEH.

Synthesis of compound m-BTP-OEH-CHO

TPBT-2Br (0.50 g, 0.57 mmol) was mixed with (3-((2-ethylhexyl)oxy)phenyl)boronic acid (0.5 g, 2.0 mmol), potassium carbonate (1.0 g, 7.2 mmol), tetrakis(triphenylphosphine)palladium (0.11 g, 0.10 mmol), toluene (30 mL), ethanol (3 mL) and water (3 mL), and stirred at 100 °C under nitrogen. After stirring for 10 h, the mixture was allowed to cool down and poured into water. The aqueous phase was extracted with ethyl acetate for three times. The organic phase was dried over sodium sulfate and concentrated under reduced pressure. The residue was purified with column chromatography over silica gel. The obtained product was then recrystallized with chloroform and methanol to yield m-BTP-OEH-CHO as orange-yellow solid (0.54 g, 85%). ^{1}H NMR (600 MHz, Chloroform-d) δ 10.01 (s, 2H), 7.50 (t, *J* = 7.9 Hz, 2H), 7.33 (d, *J* = 7.5 Hz, 2H), 7.24 (d, 2H), 7.11 (d, *J* = 8.4 Hz, 2H), 4.88-4.55 (m, 4H), 3.95 (q, *J* = 8.8, 6.7 Hz, 4H), 2.04 (h, i = 6.6 Hz, 2H), 1.79 (h, *J* = 6.3 Hz, 2H), 1.58-1.33 (m, 16H), 1.14-0.88 (m, 28H), 0.71-0.56 (m, 12H). ^{13}C NMR (151 MHz, Chloroform-d) δ 184.16, 160.05, 147.54, 145.56, 143.02, 137.48, 136.85, 133.09, 132.82, 132.80, 130.37, 129.15, 127.95, 127.92, 121.79, 116.04, 115.72, 112.52, 70.82, 55.24, 40.25, 39.45, 30.55, 29.63, 29.60, 29.14, 27.63, 23.89, 23.08, 22.74, 14.13, 13.72, 11.19, 10.03.

Synthesis of compound p-BTP-OEH-CHO

Compound p-BTP-OEH-CHO was prepared following the same procedure for m-BTP-OEH-CHO. The product was afforded as a yellow solid (0.42 g, 83%). ^{1}H NMR (600 MHz, Chloroform-d) δ 9.96 (s, 2H), 7.71 (d, *J* = 8.0 Hz, 4H), 7.12 (d, *J* = 8.2 Hz, 4H), 4.83-4.53 (m, 4H), 3.96 (d, *J* = 6.0 Hz, 4H), 2.04 (q, *J* = 6.6 Hz, 2H), 1.80 (h, *J* = 6.2 Hz, 2H), 1.59-1.34 (m, 16H), 1.14-0.88 (m, 28H), 0.67 (t, *J* = 7.5 Hz, 6H), 0.63 (dt, *J* = 10.4, 4.9 Hz, 6H). ^{13}C NMR (151 MHz, Chloroform-d) δ 184.18, 160.78, 147.54, 145.61, 142.95, 136.88, 136.68, 132.75,

132.73, 131.00, 129.12, 127.80, 127.78, 124.00, 115.34, 112.48, 70.77, 55.23, 40.23, 39.39, 30.55, 29.63, 29.60, 29.13, 27.62, 23.89, 23.09, 23.06, 22.74, 14.13, 13.71, 11.17, 10.04.

Synthesis of compound m-BTP-OEH

m-BTP-OEH-CHO (0.10 g, 0.10 mmol) was mixed with 2-(5,6-difluoro-3-oxo-2,3-dihydro-1H-inden-1-ylidene)malononitrile (100 mg, 0.38 mmol), pyridine (0.5 mL) and chloroform (30 mL). The mixture was stirred at reflux for 14 h under nitrogen. After cooling down to room temperature, the mixture was poured into methanol (150 mL) and filtered. The residue was purified by column chromatography on silica gel using petroleum ether/dichloromethane (2:1) as eluent yielding a purple solid (0.11 g, 82 %). ^{1}H NMR (400 MHz, Chloroform-d) δ 8.93 (s, 2H), 8.54 (dd, J = 10.0, 6.4 Hz, 2H), 7.75 (t, J = 7.5 Hz, 2H), 7.57 (t, J = 7.8 Hz, 2H), 7.27-7.17 (m, 6H), 5.07-4.64 (m, 4H), 4.13-3.82 (m, 4H), 2.24-2.07 (m, 2H), 1.83 (p, J = 6.0 Hz, 2H), 1.62-1.37 (m, 16H), 1.28-0.93 (m, 28H), 0.76 (ddt, J = 19.7, 9.7, 7.3 Hz, 12H). ^{13}C NMR (101 MHz, Chloroform-d) δ 185.94, 160.35, 158.59, 153.10, 151.62, 147.50, 144.95, 138.50, 137.69, 134.89, 134.53, 133.76, 133.58, 133.47, 131.35, 130.85, 122.33, 121.22, 116.56, 114.98, 114.76, 114.55, 113.64, 113.53, 112.66, 70.87, 69.67, 55.69, 40.49, 39.42, 30.56, 29.78, 29.15, 27.78, 23.92, 23.13, 14.17, 13.84, 11.18, 10.17 (d, J = 10.2 Hz).HR-MS: calculated for $C_{88}H_{82}F_4N_8O_4S_5$ [M]+, 1551.97; found: 1551.50.

Synthesis of compound p-BTP-OEH

Compound p-BTP-OEH was prepared following the same procedure as for m-BTP-OEH. The product was afforded as a purple solid (0.12 g, 86%).^{1}H NMR (600 MHz, Chloroform-d) δ 8.83 (d, *J* = 11.6 Hz, 2H), 8.58-8.43 (m, 2H), 7.72 (d, *J* = 7.8 Hz, 2H), 7.62 (d, *J* = 8.5 Hz, 4H), 7.17 (d, *J* = 8.6 Hz, 4H), 4.80 (dt, *J* = 18.9, 9.3 Hz, 4H), 4.01 (d, *J* = 11.2 Hz, 4H), 2.26-2.06 (m, 2H), 1.84 (dd, *J* = 12.5, 6.6 Hz, 2H), 1.58-1.36 (m, 16H), 1.27-0.95 (m, 28H), 0.73 (ddt, *J* = 33.6, 13.8,

7.5 Hz, 12H).^{13}C NMR (101 MHz, Chloroform-d) δ 185.78, 161.56, 158.83, 153.01, 151.92, 147.44, 144.65, 138.91, 137.66, 134.86, 134.41, 133.68, 133.03, 131.76, 131.23, 124.41, 120.91, 115.92, 114.83, 114.65, 113.67, 113.56, 112.59, 112.40, 70.97, 69.21, 55.65, 40.45, 39.34, 30.54, 29.73, 29.13, 27.73, 23.88, 23.20, 23.10, 22.86, 14.14, 13.78, 11.16, 10.11. HR-MS: calculated for $C_{88}H_{82}F_4N_8O_4S_5$ [M]+, 1551.97; found: 1551.50.

3. Device Fabrication

The OSCs were fabricated with a conventional structure of ITO/PEDOT:PSS/Active layer/PDINO/Ag. First, ITO-coated glass was cleaned with deionized water, acetone, and isopropyl alcohol under ultrasonication for sequentially 15 mins. Second, the surface of ITO-coated glass was treated in an ultraviolet-ozone chamber for 15 min. A thin layer of PEDOT:PSS (Baytron P VP AI 4083) was deposited on the ITO substrate at 4300 rpm for 20 s and then dried at 150 ℃ for 20 mins in air. Then the substrates were transferred to a glovebox filled with nitrogen. The PM6:m-BTP-OEH or PM6:p-BTP-OEH was dissolved in chloroform with 1-Chloronaphthalene (1-CN) as the additive. The active layer was spun onto the PEDOT:PSS layer at 2000 rpm for 30 s, and then the films were treated with thermal annealing. After cooled down, the methanol solution of PDINO (2 mg/mL) was spin-coated on the top of the active layer at 3000 rpm for 20 s. Finally, Ag electrode with the thickness of 150 nm was evaporated under 2×10^{-6} Pa. The active area of device was 4 mm^2.

4. Figures and Tables

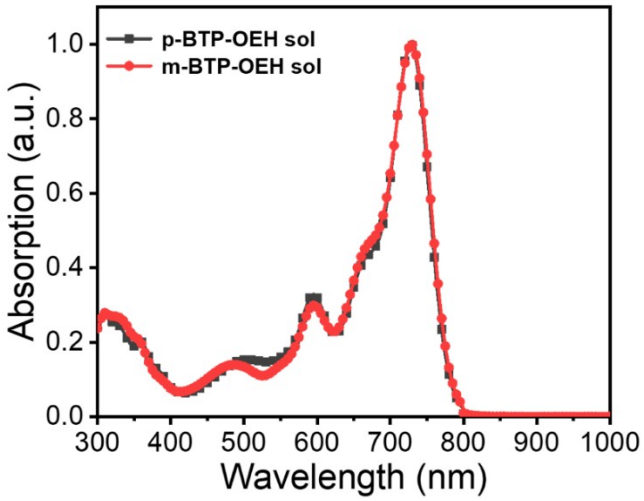

Figure S1. Normalized UV-vis absorption spectra of p-BTP-OEH and m-BTP-OEH in CF solution.

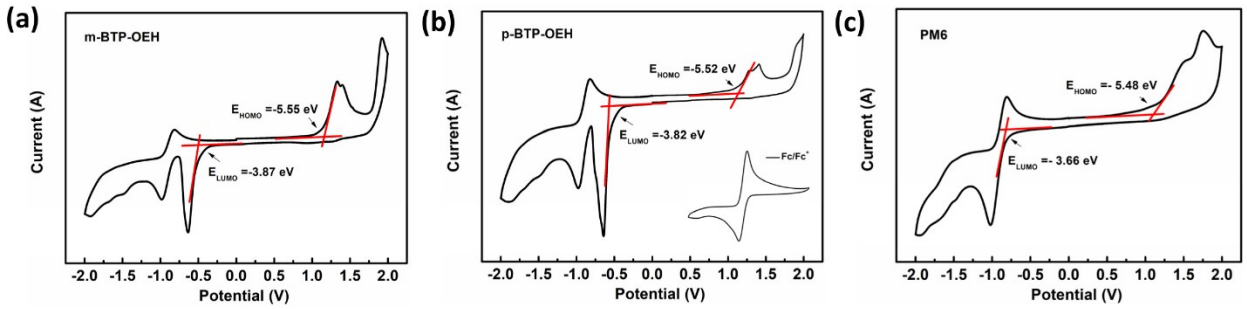

Figure S2. Cyclic voltammograms of m-BTP-OEH, p-BTP-OEH and PM6. The HOMO and LUMO positions are determined by the point of intersection using two tangent lines at the onsets of oxidation or reduction waves. The equation of $E_{LUMO}/H_{OMO} = -e(E_{red}/_{ox}+4.39)$ (eV) was used to calculate the LUMO and HOMO levels (the redox potential of Fc/Fc+ is found to be 0.41 V).

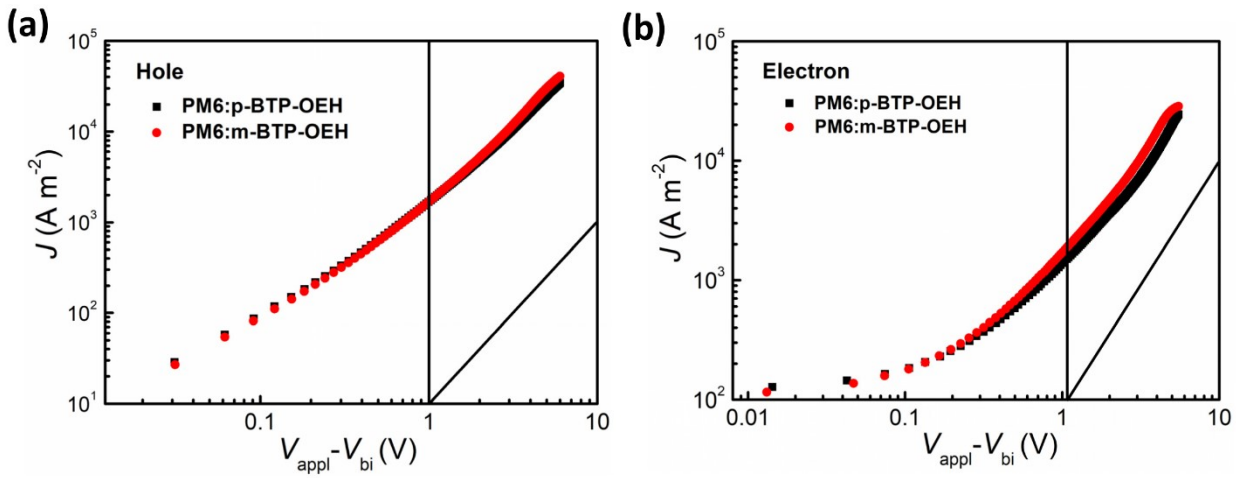

Figure S3. The *J*-V plots for the a) hole-only and b) electron-only devices based on PM6:m-BTP-OEH and PM6:p-BTP-OEH, respectively.

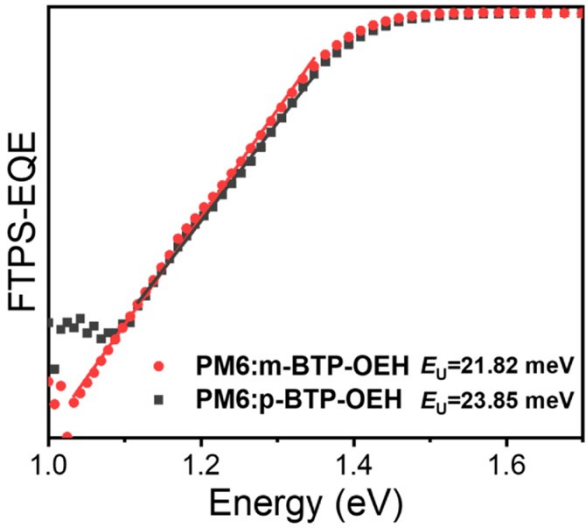

Figure S4. FTPS-EQEs of PM6:m-BTP-OEH and PM6:p-BTP-OEH-based OSCs at the absorption onset and their Urbach energy (E_U) values. For disordered semiconductors that generally produce localized states extending into the bandgap, the optical absorption coefficient (α(E)) inthe low photon energy range follows the Urbach rule following $\alpha(E) = \alpha_0 e^{(E - E_g)/E_U}$,

where α_0 is the optical absorption coefficient at the band edge, E is the photon energy and E_U is the Urbach energy.

Table S1 Performance of the OSCs with different PM6 (D)/ m-BTP-OEH (A) ratios.

D:A	V_{OC} (V)	J_{sc} (mA/cm^2)	FF (%)	PCE (%)
1:1	0.862	25.50	72.15	15.92
1:1.2	0.858	25.48	73.40	16.11
1:1.4	0.862	25.50	71.09	15.68

Table S2 Photovoltaic performance of solar cells based on PM6:m-BTP-OEH (1:1.2, w/w) blend films with different TA temperature.

TA (℃)	V_{OC} (V)	J_{sc} (mA/cm^2)	FF (%)	PCE (%)
80	0.857	25.65	73.52	16.22
100	0.855	26.30	74.18	16.75
120	0.850	26.32	74.06	16.62

Table S3 Photovoltaic performance of solar cells based on PM6:m-BTP-OEH (1:1.2, w/w) blend films with different additive contents.

CN (vt%)	V_{OC} (V)	J_{sc} (mA/cm^2)	FF (%)	PCE (%)
0.3	0.856	26.46	75.96	17.27
0.5	0.856	26.84	78.41	18.02
0.7	0.841	26.23	76.54	16.94

Table S4 Photovoltaic performance of solar cells based on PM6:m-BTP-OEH (1:1.2, w/w, 0.5% CN) blend films with different TA temperature.

TA (°C)	V_{OC} (V)	J_{sc} (mA/cm^2)	FF (%)	PCE (%)

80	0.856	26.49	75.69	17.23
100	0.856	26.84	78.41	18.02
120	0.850	26.67	76.28	17.35

Table S5. Detailed photovoltaic parameters of the PM6:p-BTP-OEH based devices by optimal conditions under the illumination of AM 1.5 G, 100 mW cm^{-2}.

Active layer	V_{oc} (V)	J_{sc} (mA/cm^2)	FF (%)	PCE (%)
PM6:p-BTP-OEH	0.890	26.09	75.68	17.59
	0.880	26.24	74.95	17.36
	0.884	26.02	75.97	17.49
	0.883	26.03	76.03	17.49
	0.882	25.96	76.39	17.51
	0.887	25.84	76.20	17.48
	0.882	26.23	75.98	17.59
	0.889	26.22	75.40	17.58
	0.884	26.27	75.88	17.63
	0.882	26.11	75.73	17.45
	0.885	26.10	75.82	17.52
Average	0.885±0.003	26.10±0.14	75.82±0.39	17.52±0.08

Table S6. Detailed photovoltaic parameters of the PM6:m-BTP-OEH based devices by optimal conditions under the illumination of AM 1.5 G, 100 mW cm^{-2}.

Active layer	V_{oc} (V)	J_{sc} (mA/cm^2)	FF (%)	PCE (%)
PM6:m-BTP-OEH	0.855	27.03	77.32	17.88
	0.854	27.04	77.77	17.97
	0.857	26.82	77.96	17.93
	0.856	26.84	78.41	18.02
	0.855	26.92	78.10	17.98
	0.858	27.01	77.59	17.99
	0.856	26.98	77.56	17.92
	0.856	26.89	77.78	17.92
	0.856	27.00	77.92	18.01
	0.854	26.85	77.73	17.85
	0.856	26.94	77.81	17.95
Average	0.856±0.002	26.94±0.08	77.81±0.29	17.95±0.05

Table S7. Contact angle and miscibility parameters of blend films.

Film	θ_{water} (°)	$\theta_{glycerol}$ (°)	γ (mN m^{-1})	$\chi_{D,A}$ (κ)
PM6	105.64	86.02	22.0	
m-BTP-OEH	88.87	85.49	29.1	0.496
p-BTP-OEH	91.11	83.81	28.8	0.457

Table S8. Summary of the GIWAXS parameters for the neat acceptor films and blend films

Film	(010)			(100)		
	q (Å^{-1})	d^{a} (Å)	CCL^{b} (Å)	q (Å^{-1})	d^{a} (Å)	CCL^{b}(Å)
m-BTP-OEH	1.74	3.61	0.26	0.27	22.92	22.17
p-BTP-OEH	1.70	3.69	0.27	0.26	23.97	20.78
PM6:m-BTP-OEH	1.75	3.58	0.32	0.30	21.43	17.89
PM6:p-BTP-OEH	1.74	3.61	0.35	0.29	21.88	16.10

5. NMR Spectra

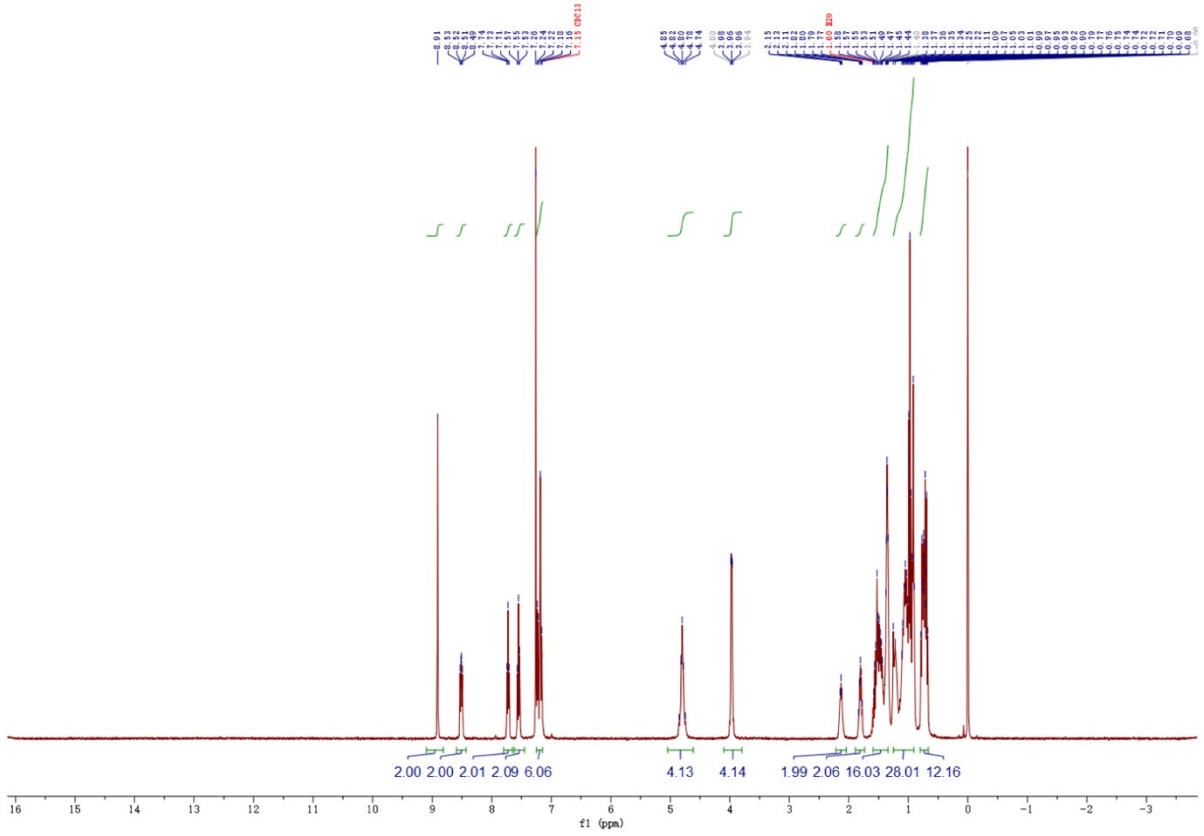

Figure S5. ^{1}H NMR (400 MHz) of compound m-BTP-OEH.

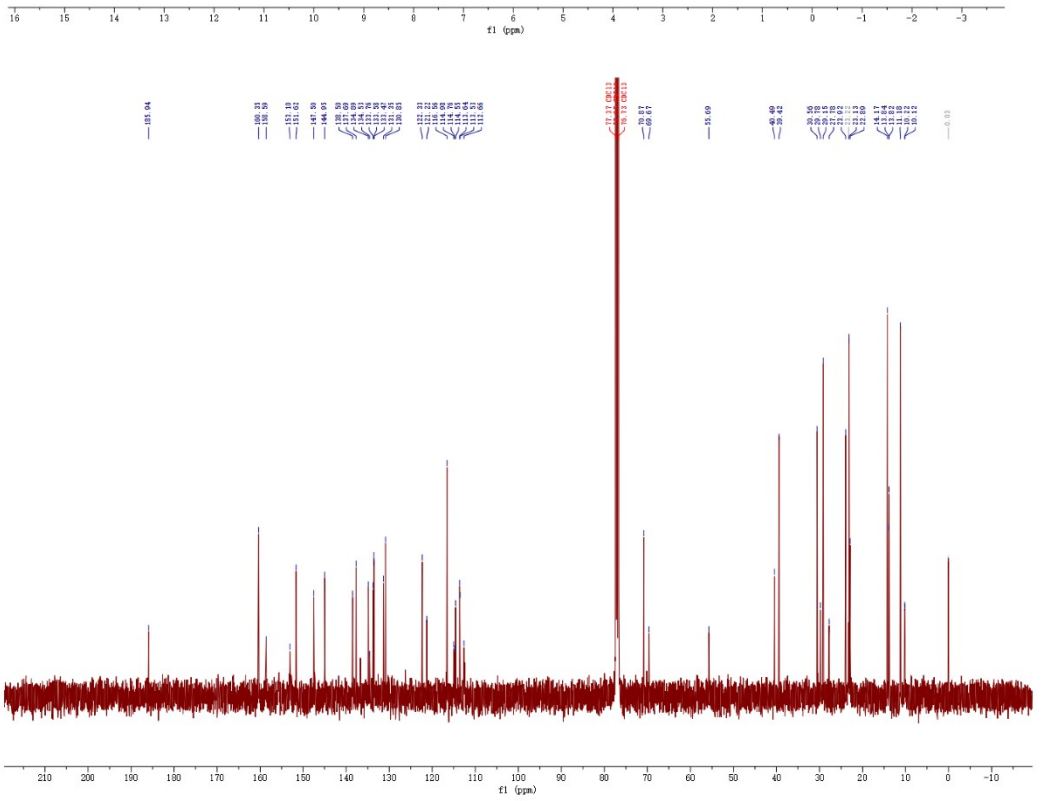

Figure S6. ^{13}C NMR (101 MHz) of compound m-BTP-OEH.

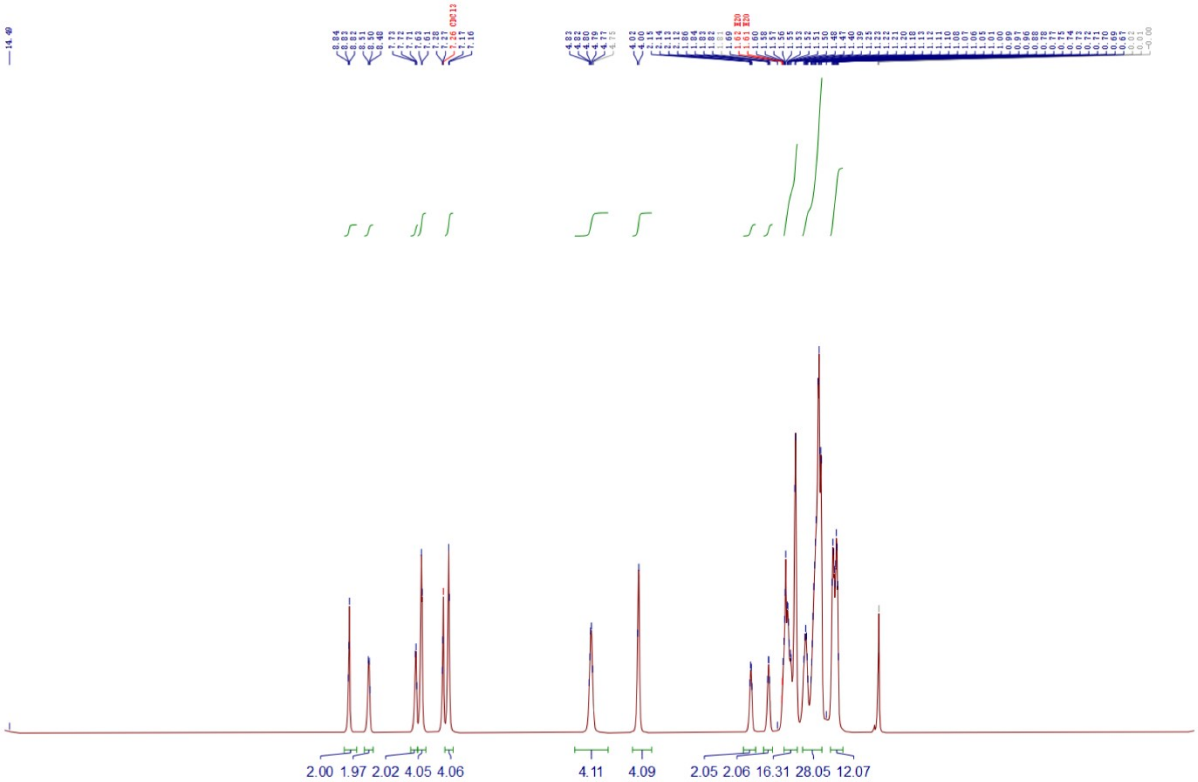

Figure S7. ^{1}H NMR (600 MHz) of compound p-BTP-OEH.

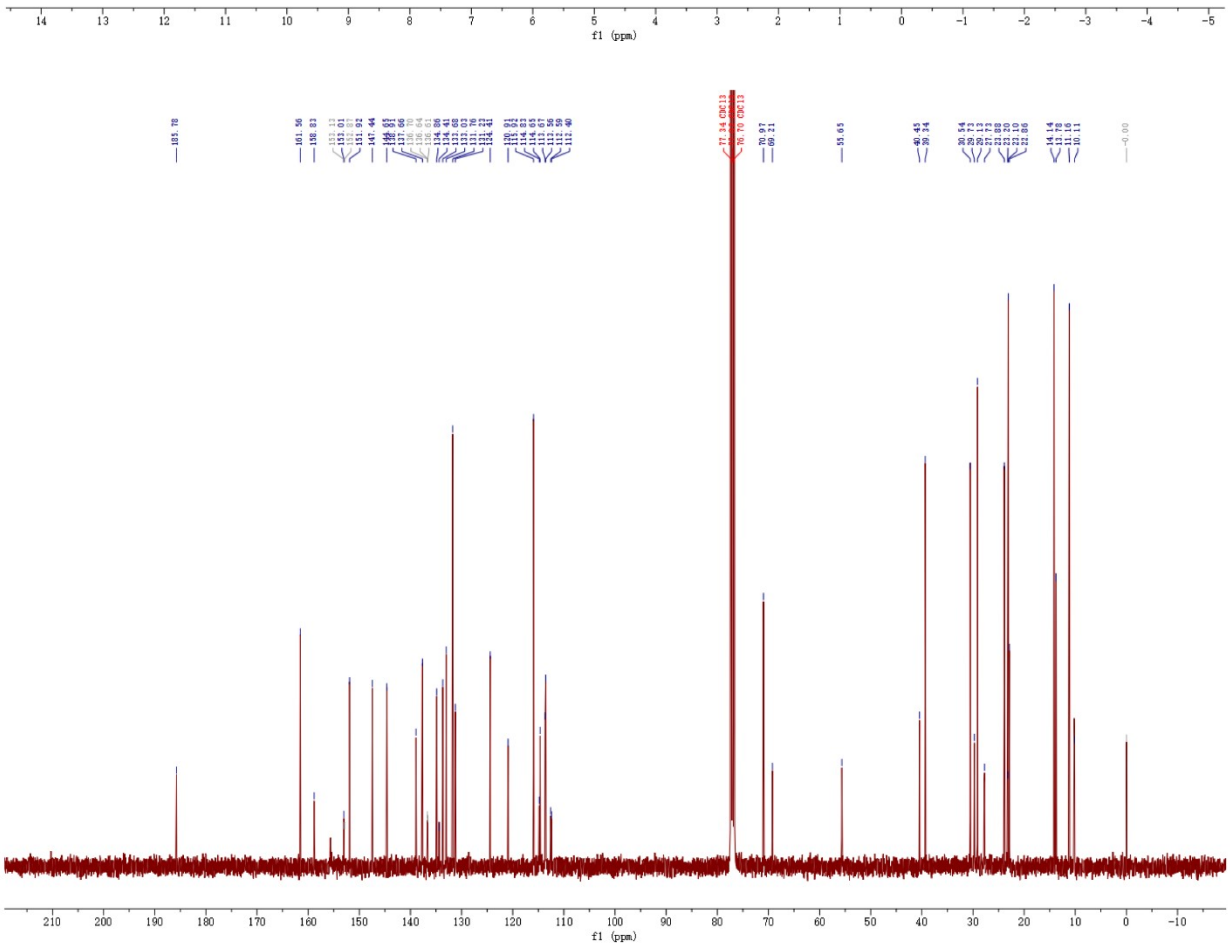

Figure S8. ^{13}C NMR (101 MHz) of compound p-BTP-OEH.

6. High-Resolution Mass Spectra

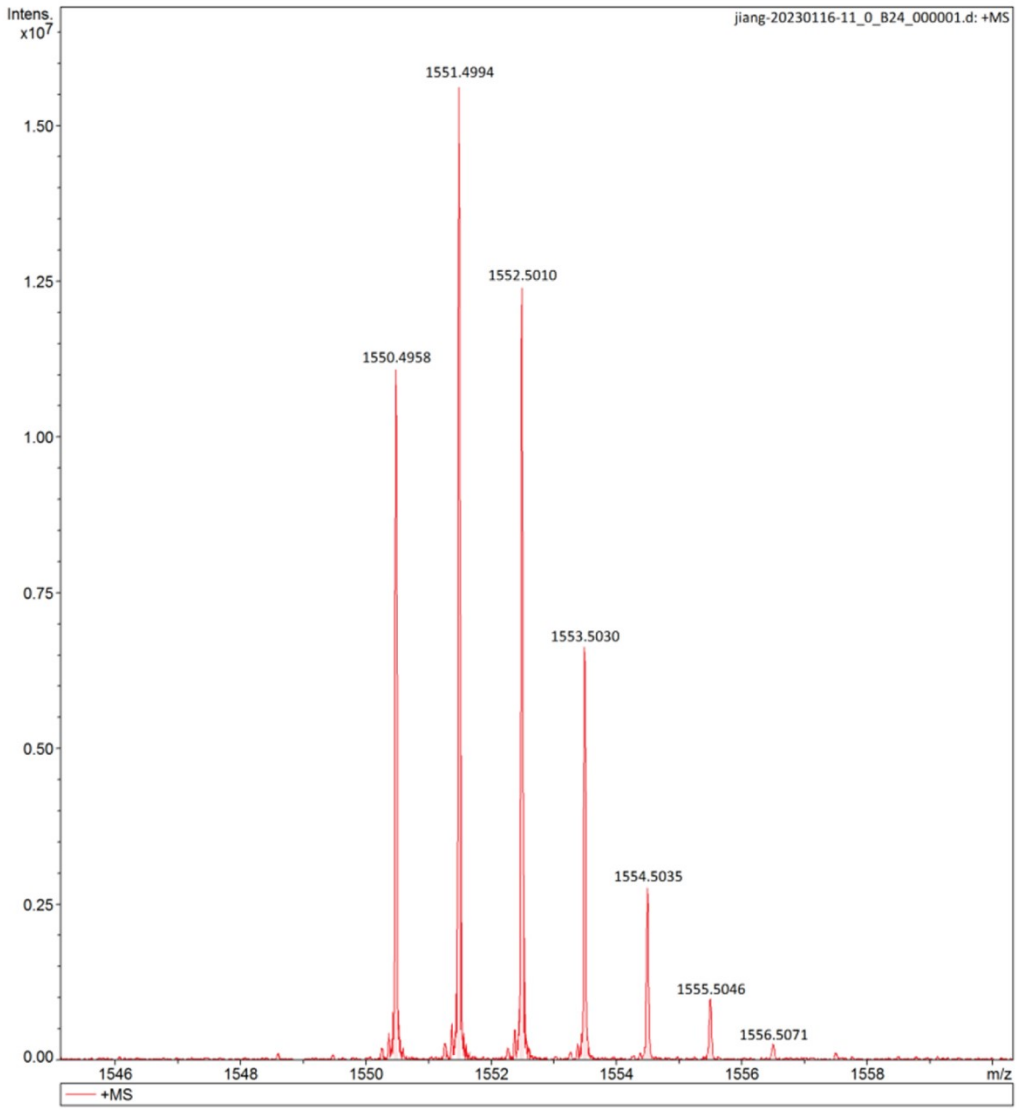

Figure S9. HR-MS spectrum of compound m-BTP-OEH.

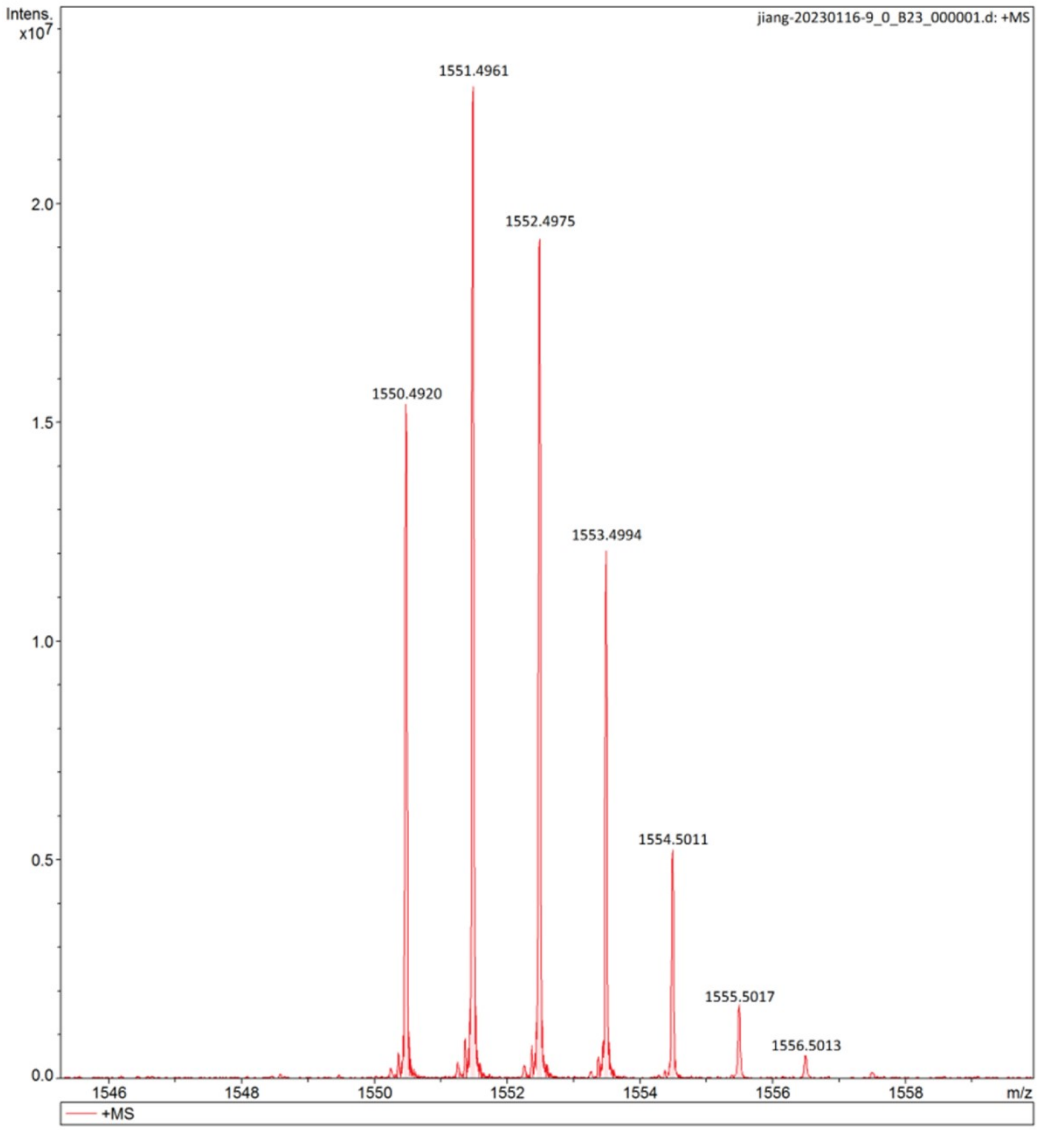

Figure S10. HR-MS spectrum of compound p-BTP-OEH.

7. References

1. Z. Li, C. Jiang, X. Chen, G. Song, X. Wan, B. Kan, T. Duan, E. A. Knyazeva, O. A. Rakitin and Y. Chen, *J. Mater. Chem. C*, 2023, **11**, 6920-6927.